



HAL
open science

Unraveling the effect of low Cu₂O loading on P25 TiO₂ and its self-reduction during methanol photoreforming

Fernando Plascencia-Hernández, Elim Albiter, Mohamed Nawfal Ghazzal, Christophe Colbeau-Justin, Hynd Remita, Heriberto Pfeiffer, Miguel Valenzuela

► To cite this version:

Fernando Plascencia-Hernández, Elim Albiter, Mohamed Nawfal Ghazzal, Christophe Colbeau-Justin, Hynd Remita, et al.. Unraveling the effect of low Cu₂O loading on P25 TiO₂ and its self-reduction during methanol photoreforming. *Inorganic Chemistry Communications*, 2023, 158, pp.111541. 10.1016/j.inoche.2023.111541 . hal-04250710v2

HAL Id: hal-04250710

<https://hal.science/hal-04250710v2>

Submitted on 19 Nov 2023

HAL is a multi-disciplinary open access archive for the deposit and dissemination of scientific research documents, whether they are published or not. The documents may come from teaching and research institutions in France or abroad, or from public or private research centers.

L'archive ouverte pluridisciplinaire **HAL**, est destinée au dépôt et à la diffusion de documents scientifiques de niveau recherche, publiés ou non, émanant des établissements d'enseignement et de recherche français ou étrangers, des laboratoires publics ou privés.

Unraveling the effect of low Cu₂O loading on P25 TiO₂ and its self-reduction during methanol photoreforming

Fernando Plascencia-Hernández^{1,2,4*}, G. Valverde-Aguilar^d, M.N. Ghazzal³, C. Colbeau-Justin³, H. Remita³, Heriberto Pfeiffer⁴, M.A. Valenzuela^{3*}

¹Centro de Investigación en Ciencia Aplicada y Tecnología Avanzada Unidad Legaria, Instituto Politécnico Nacional. Legaria 694, Col. Irrigación, 11500, CDMX, México.

²Lab. Catálisis y Materiales. ESQIE- Instituto Politécnico Nacional. Zacatenco, 07738 México, CDMX, México.

³Lab. Chimie Physique, CNRS UMR 8000, Univ. Paris-Sud, 91405 Orsay, France

⁴Instituto de Investigaciones en Materiales, Universidad Nacional Autónoma de México. Circuito exterior s/n, Ciudad Universitaria, Del. Coyoacán, CP 04510, CDMX, México.

* Corresponding authors: fernandoplascenciah@gmail.com; mavalenz@ipn.mx

^d deceased

ABSTRACT

The use of noble metal-free catalysts is one of the most attractive routes for the photocatalytic production of H₂ under sunlight. In that sense, recently, copper compounds have had a growing interest in this subject. Particularly, Cu₂O/semiconductor composites have shown enhanced photocatalytic activity in comparison with single compounds. In the present work, different Cu_xO (X=1, 2)/TiO₂ composites, with Cu_xO weight ratio from 1 to 0.05 respect to TiO₂ source, were obtained through aqueous mixture. Firstly, the Cu_xO particles were obtained by chemical reduction method at room temperature, and after, mixed with commercial Degussa (Evonik) P25 TiO₂, through the dispersion of each one in a water:ethanol solution. All these materials were characterized by different techniques, such as X-ray diffraction (XRD), scanning electron microscopy (SEM), X-ray photoelectron spectroscopy (XPS), diffuse reflectance spectroscopy (DRS) and time resolved microwave conductivity (TRMC). Through the DRS technique, it was observed that composites possessed two separated optical absorption bands in UV and visible regions, confirming the physical interaction between both oxides and an extended optical activity. Charge carrier dynamics was studied by TRMC. Finally, the photocatalytic activity of the materials was evaluated for H₂ production by methanol photoreforming at batch approach, using simulated solar light. The best H₂ production was obtained with the 0.1-Cu/Ti composite, moreover its photoperformance was similar after three evaluation cycles, suggesting high stability under the reaction conditions. During irradiation of all the composites in the reactive system, the color of the solution changed from slight yellow to deep purple, which was attributed to the change of the copper oxidation states.

Keywords: Cu₂O/TiO₂ composites, methanol photoreforming, copper oxides reduction, simulated solar light.

1. Introduction

The global population growth and the corresponding energy demand are leading to the excessive fossil fuel consumption, increasing the greenhouse gases emission. This situation is being a critical factor for the increment in the global planet-warming. Therefore, the transition toward carbon-free energy sources like hydrogen (H_2) could be a reasonable alternative to solve the energy demand and the associated environmental impact. Hydrogen possesses attractive properties that make it the one of best candidates to substitute the current fuels; it has the highest energy content of any fuel (141.88 MJ/kg as gaseous state), non-toxic and clean, since water is the only emission after its combustion [1], [2]. Concerning to H_2 production, there is a large amount of information devoted to conventional routes as thermochemical, biomass pyrolysis, and solar approaches [2]–[4]. Especially, solar energy conversion to H_2 seems to be one of the most suitable ways in the near future, by using photochemical, photoelectrocatalytic or photocatalytic processes [3].

The photocatalytic H_2 generation can be obtained mostly by two different approaches: i) photocatalytic water splitting [5] and ii) photocatalytic reforming of organic compounds [6]. The first method relates to the capability of water to be reduced and oxidized, by reacting with photogenerated electrons and positive holes during semiconductor irradiation, which can possess selected co-catalysts. The second approach is based on the ability of some organic species, to donate electrons to the positive holes, after semiconductor excitation, then, generating protons that can be reduced to hydrogen by the photogenerated electrons.

The photoreforming of organic compounds like methanol, ethanol or glycerol in aqueous solution is an attractive process, which occurs coupling the organic compound oxidation and proton reduction, preventing the back-reaction between H_2 and O_2 [7]. Undoubtedly, the most important aspects to consider in the photoreforming are the selection of a suitable catalyst, the type of organic compound employed and the use of co-catalysts [6], [8]. Titanium dioxide (TiO_2 , n-type semiconductor) has been the most studied material for this reaction, due to its extraordinary properties: high oxidative power, chemical stability,

cheap and friendly to the environment [9] [10]. Furthermore, it has been reported that the mixture of rutile and anatase phases of this oxide is more photoactive than the presence of single phase only. The disadvantages of TiO_2 are the high value of its band gap (generally reported as $E_g = 3.2$ eV), which demands UV-light for its activation [6], [11] and its fast recombination rate of photogenerated electron–hole pairs [8].

For this reason, several options have been considered to improve the photocatalytic activity of TiO_2 under visible light, among them: (i) surface modification via organic materials, (ii) band gap modification by nonmetals, (iii) metals doping and (iv) semiconductor coupling [6], [8], [11]. The combination of n-type semiconductor with a p-type semiconductor, as copper oxides (CuO , Cu_2O), forms a heterojunction, considered as efficient method to separate the photoinduced electrons and holes due to the effect of the inner electric field [12]. The suitable properties of Cu_2O such as its band gap of 2.0 eV, a wide absorption coefficient in visible spectrum and virtual non-toxicity, has been widely explored by several research groups on applications as, solar cells, gas sensor and water splitting, among others [13]. Indeed, the $\text{Cu}_2\text{O}/\text{TiO}_2$ heterojunctions have shown promising photocatalytic results in several reactions [14], [15]. Their staggered gap (type-II) enables the photogenerated charge separation in two distinct semiconductors [16]. Thus, the photogenerated electrons can be transferred from the Cu_2O conduction band (CB) to TiO_2 , and the holes can be transferred from the TiO_2 valence band (VB) to the Cu_2O VB [17], [18].

Conversely, the reactor configuration represents an important factor in the photocatalytic performance. The use of batch reactors in photocatalysis allows to exploring the evolution of the reactants and products concentration, as well as the reaction kinetics, in an easy way and with good temperature control, avoiding the influence of internal and external diffusion [19] [20].

In this work, Cu_2O - CuO particles were combined to P25 TiO_2 with different weight ratio (Cu_2O - $\text{CuO}/\text{TiO}_2 = 1, 0.5, 0.1$ and 0.05) via wet mixture, to study the synergic effect during their photocatalytic

performance in the methanol photoreforming. Surprisingly, during the irradiation with solar simulator, simultaneously methanol photoreforming and self-reduction of copper oxides to metallic copper (Cu^0) were carried out, suggesting a high reductive environment, being positive effect over the H_2 generation. This self-reduced process was explained based on several combined factors of the system $\text{Cu}_x\text{O-TiO}_2$ and reaction conditions.

2. Materials and Methods

2.1 Materials

Copper (II) chloride (CuCl_2 ; 97%), sodium hydroxide (NaOH ; 98.2%), L-ascorbic acid (99.5%), Polivinilpilorridone (PVP; M_w 40,000), titanium dioxide P25 Degussa (P25 TiO_2 ; 99.5%) were purchased from Aldrich and used without further purification. Aqueous solutions were prepared using deionized water (Milli-Q with 18.6 $M\Omega$), ethanol reagent grade (denatured) and methanol reagent grade.

2.2 Synthesis of Cu_xO ($X=1, 2$) polyhedral microparticles

Cu_xO polyhedral particles were synthesized at room temperature under chemical reduction route with slight modifications [21]. Sodium hydroxide solution (1M, 40 mL) was prepared and stirred vigorously. Copper chloride solution (0.15 M, 40 mL) was added dropwise to the sodium hydroxide solution, and stirred during 15 minutes. After that, a 60 mL of PVP and L-ascorbic acid solution (1.42 weight ratio) was added suddenly in the last solution, and it was stirred for 30 minutes. The obtained Cu_xO polyhedral particles were washed three times with a 1:1 water:ethanol solution, and dry under air for storage.

2.3 Synthesis of $\text{Cu}_x\text{O/TiO}_2$ composites

Cu_xO polyhedral particles and P25 TiO_2 nanoparticles were dispersed separately in two ethanol:water 0.6:1 v:v solutions in both cases. P25 TiO_2 solution was added dropwise to the Cu_xO solution under

vigorous stirring until to obtain a homogeneous solution. Then, it was dried in air and the final powder was stored. Under this procedure, four composites were synthesized with the nominal weight ratio showed in Table 1.

Table 1. Nominal composition of the composites

Composite	Weight ratio (Cu _x O/P25 TiO ₂)
1-Cu/Ti	1
0.5-Cu/Ti	0.5
0.1-Cu/Ti	0.1
0.05-Cu/Ti	0.05

2.4 Characterization techniques

The characterization of the composites was accomplished through several techniques. X-ray diffraction (XRD) were recorded from 15 to 80°, with a scan rate of 2° min⁻¹, using a Rigaku ULTIMA IV diffractometer in Bragg–Brentano geometry (Cu-K_{α1} radiation, $\lambda = 1.540562 \text{ \AA}$) and nickel filter. Then, the morphology and particle size were determined by scanning electron microscopy (SEM), which was carried out on a JEOL 7800F microscope without any previous treatment. X photoelectron spectroscopy (XPS) measurements were performed using a K–Alpha from Thermo Fisher Scientific X-ray photoelectron spectrometer with a monochromatic Al K_α X-ray source (1486.6 eV) and a base pressure of 1x10⁻⁹ Torr in the analytical chamber. The binding energy values were calibrated by contaminant carbon using the C 1s position at 285 eV, and all the reference binding energies were obtained from NIST X-ray Photoelectron Spectroscopy Database. UV–vis diffuse reflectance spectroscopy (DRS) was measured on a GBC Cintra 20 spectrometer on the range of 200-800 nm. Finally, charge-carrier dynamic experiments were carried out through Time Resolved Microwave Conductivity (TRMC), using an incident microwave generated by a Gunn diode of the K_α band at 30 GHz. As a pulse light source, a laser (EKSPLA, NT342B)

tunable in the range between 220 and 2000 nm, equipped with an optical parametric oscillator (OPO) was used, delivering 8-ns FWHM pulses with a frequency of 10 Hz. Three excitation wavelengths were selected 360, 470 and 520 nm with a light energy density of 2.6 mJ cm^{-2} .

2.5 Photocatalytic evaluation

The photocatalytic evaluation was carried out as follows. First, the P25 TiO₂ Degussa, Cu_xO particles and Cu_xO/TiO₂ composites were tested through a home-made batch reaction system, using a methanol water mixture (MeOH:H₂O, 1:10; v:v) as a reaction medium. The concentration of the photocatalyst was fixed at 1 g L^{-1} in the reaction volume. At the beginning, oxygen inside of the reactor was removed by bubbling N₂ gas for 15 min. After that, the mixture was stirred in dark condition for 30 minutes, to reach adsorption-desorption equilibrium between the catalyst and the methanol-water solution. Then, the reactor was irradiated using Hg-Xe lamp light source with a power of 150 W for 8 h. The H₂ production was followed each hour using a gas chromatograph Perkin Elmer Clarus 480 with a TCD detector. Each evaluation was performed three times. Under similar procedure, water splitting reaction and the effect of the concentration of the photocatalyst were studied with the composite that showed the higher photoactivity. Furthermore, to assess the stability of this composite, cyclic experiments were performed, in which the photocatalyst was recovered by centrifugation after the first evaluation and redissolved in a fresh methanol-water solution (MeOH:H₂O, 1:10), and following with the following evaluation.

3. Results

The diffraction patterns of the synthesized materials are displayed in Figure 1. In the copper particles, the diffraction peaks located at 29.6, 36.5, 42.4, 52.6, 61.6, 73.7 and 77.5° of 2θ correspond to the cuprite structure of Cu₂O phase, according with JCPDS No. 01-073-6371, as expected. Furthermore, small peaks located at 35.7 and 38.3° were detected as well, which can be attributed to CuO phase (JCPDS No. 00-

005-0667). Hence, the copper particles are composed by both, Cu_2O and CuO , the last one in less proportion respect to the Cu_2O . For the Cu_2O particles, the crystallite size (D) was determined using the XRD peak located at 36.5° , through Scherrer's equation (Equation 1), where $\lambda=1.5406 \times 10^{-10}$ m, B is the peak width, and θ represents the Bragg angle of the peak used. Thus, the crystallite size of the Cu_2O particles was calculated as 19 nm.

$$D = \frac{0.9\lambda}{B \cdot \cos\theta} \quad (1)$$

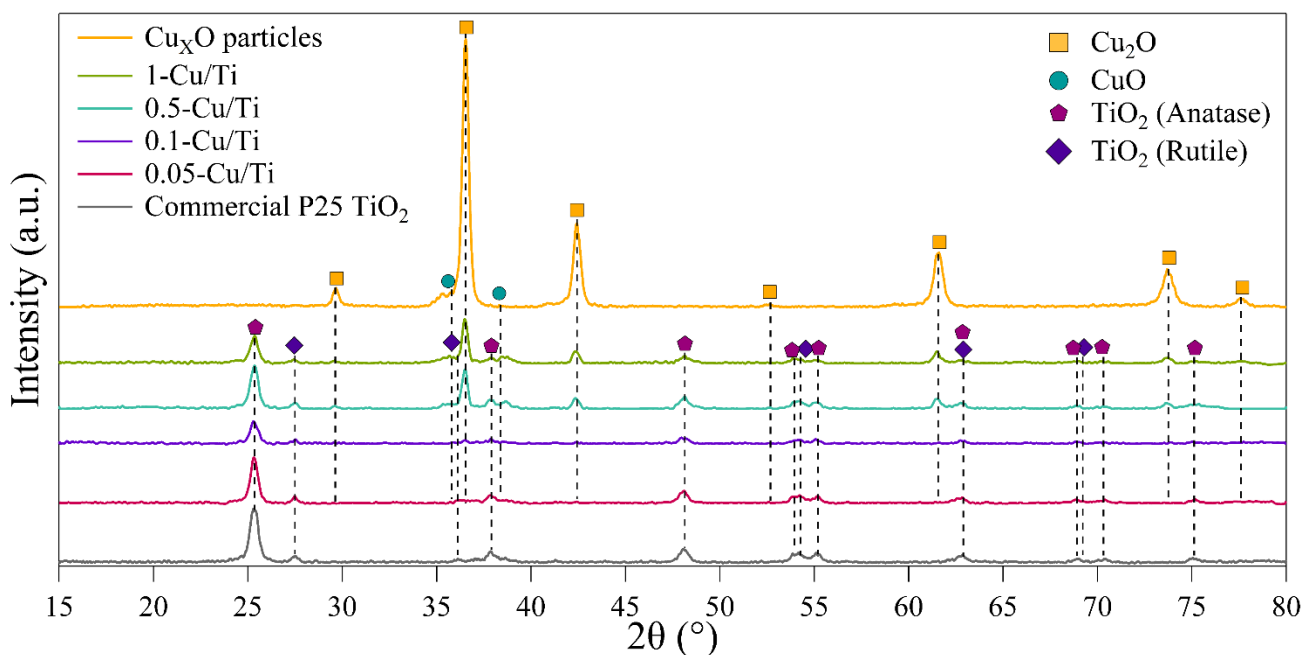


Figure 1. X-ray diffraction patterns of Cu_xO particles, $\text{Cu}_x\text{O}/\text{TiO}_2$ composites and commercial P25 TiO_2 .

As both, Cu_2O and CuO , are presented in the copper particles, they were labeled as Cu_xO . In the $\text{Cu}_x\text{O}/\text{TiO}_2$ composites, moreover of the peaks attributed to the Cu_xO particles, they showed the typical patterns corresponding to the anatase (A) and rutile (R) phases from P25 TiO_2 , according to the JCPDS No. 00-021-1272 and No. 01-070-7347 cards, respectively, which it was confirmed with the XRD pattern of commercial P25 TiO_2 . It is worth noting the significant decrease in the highest Cu_2O diffraction peak intensity (36.5°), in agreement to the decrease of the Cu/Ti weight ratio in the composites. Any additional compound was found.

After the structural characterization, microstructural properties were determined via SEM technique, and showed in the Figure 2. According to the first image (Figure 2A), the Cu_xO particles present a polyhedral morphology, as it was expected, with some agglomeration regions. The average size of these particles was calculated measuring 100 particles, and determined as 196 nm. For the Cu/Ti composites, in general, it seems that the Cu_xO particles are surrounded by P25 TiO_2 nanoparticles randomly. The micrograph of the 1-Cu/Ti composite (Figure 2B), containing the highest Cu_xO content, enables to identify Cu_xO particles and P25 TiO_2 , whose primary particle size has been reported as 21 nm. Figure 2C shows the 0.5-Cu/Ti particles, where the Cu_xO particles remain visible, although their concentration is lower, compared to the previous case. On the contrary, 0.1-Cu/Ti and 0.05-Cu/Ti composites show in Figure 2D and 2E, respectively, Cu_xO polyhedral particles were not identified, due to their low proportion respect to the P25 TiO_2 . However, the same configuration is expected, as it was noted in the 0.1-Cu/Ti and 0.05-Cu/Ti composites, where Cu_xO particles are surrounded by P25 TiO_2 nanoparticles.

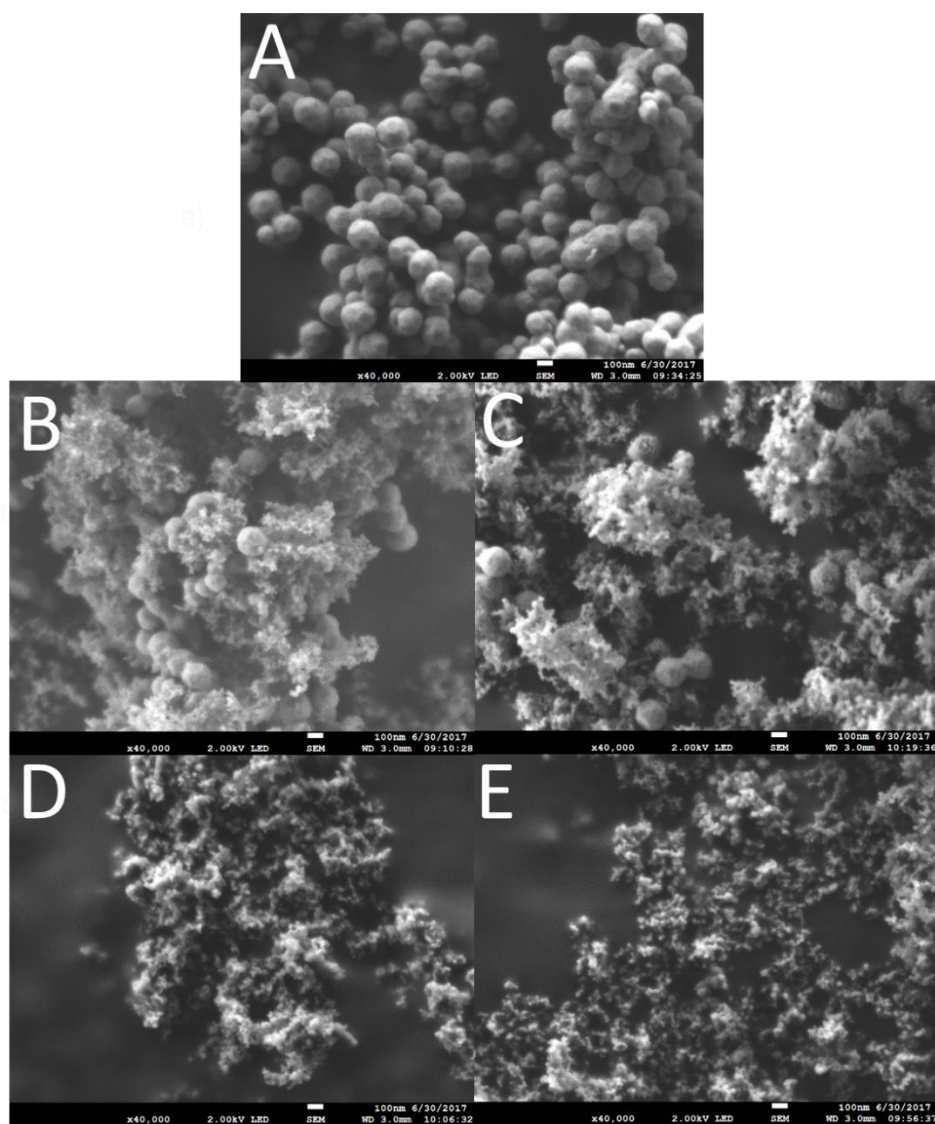


Figure 2. SEM images of Cu_xO particles A) and the 1-Cu/Ti B), 0.5-Cu/Ti C), 0.1-Cu/Ti D) and 0.05-Cu/Ti E) composites.

The XPS measurements were performed to determine the surface composition and Cu species presented in the 0.1-Cu/Ti and 0.05-Cu/Ti composites, as shown in Figure 3. The survey spectra (Figure 3A) displayed four main elements: C, Ti, O, and Cu. The presence of carbon could have resulted from hydrocarbons pollution from the XPS instrument itself or the adsorbed hydrocarbon from the air, and it was taken as standard signal reference to the other peaks. The binding energy (BE) at 458.2 and 464.0 eV

were assigned to Ti 2p_{3/2} and Ti 2p_{1/2} (Figure 3B), respectively. The separation measured between the Ti 2p_{3/2} and Ti 2p_{1/2} peaks was 5.8 eV, which correspond to the BE separation observed for stoichiometric TiO₂ [22]. On the Figure 3C, it was plotted the signals which corresponds to the oxygen O_{1s}. After deconvolution of this region, two peaks were observed at 529.6 and 530.9 eV in both composites, which were assigned as an interaction between Cu-O in CuO, and the presence of Cu(OH)₂, respectively. The first peak corroborates the presence of CuO in the surface of the Cu_xO particles, determined by the XRD characterization, while the second one should be remained secondary specie formed during the Cu_xO synthesis process. Figure 3D shows the spectrum of the Cu 2p region in the 0.1-Cu/Ti composite. As in the previous case, after the deconvolution of the Cu 2p spectrum, several peaks were identified. The peaks located at 932.4 and 952.4 eV, corresponded to the Cu₂O specie, and they were assigned to Cu2p_{3/2} and Cu2p_{1/2}, respectively. By other hand, the peak located at 953.7 eV, can be designated as Cu2p_{1/2} of CuO. Additionally, satellite peaks were observed at 934.2, 941.1 and 943.7 eV. These satellite peaks have been reported at the existence of fully oxidized copper, as CuO, and assigned to Cu2p_{3/2}. In the 0.05-Cu/Ti composite (Figure 3E), the same set of peaks were found in a similar position than those detected in the 0.1-Cu/Ti composite. The peaks located at 932.3 and 952.4 eV were associated to Cu₂O and assigned to Cu2p_{3/2} and Cu2p_{1/2}, respectively. The same satellite CuO peaks were found at 934.2, 941.0 and 943.6 eV, although the peak at 934.2 eV, associated to CuO 2p_{3/2}, displayed a higher intensity, with respect at the observed one in the 0.1-Cu/Ti composite. Table 2 shows the experimental surface atomic composition percent of each element in both composites, compared with the theoretical atomic composition, based on the weight ratio considered in the synthesis of the composites. For oxygen, the atomic composition is similar in both, theoretical and experimental values. However, theoretical titanium and copper percentages were different respect to the experimental results. For the experimental values, in the titanium case, the atomic percentage was lower, meanwhile the copper percentage was higher, both respected to the

theoretical value, on each composite. However, if the experimental values of the atomic percentages are compared of each element between the composites, in all the cases, the values are essentially the same, which means that, at least on the surface, the composition of these composites are similar.

Table 2. Experimental percent of the surface atomic composition

Element	0.1-Cu/Ti		0.05-Cu/Ti	
	Theoretical	Experimental	Theoretical	Experimental
O1s	64.9	64.1	65.8	64.5
Ti2p	31.6	29.2	32.4	29.0
Cu2p	3.5	6.7	1.8	6.5

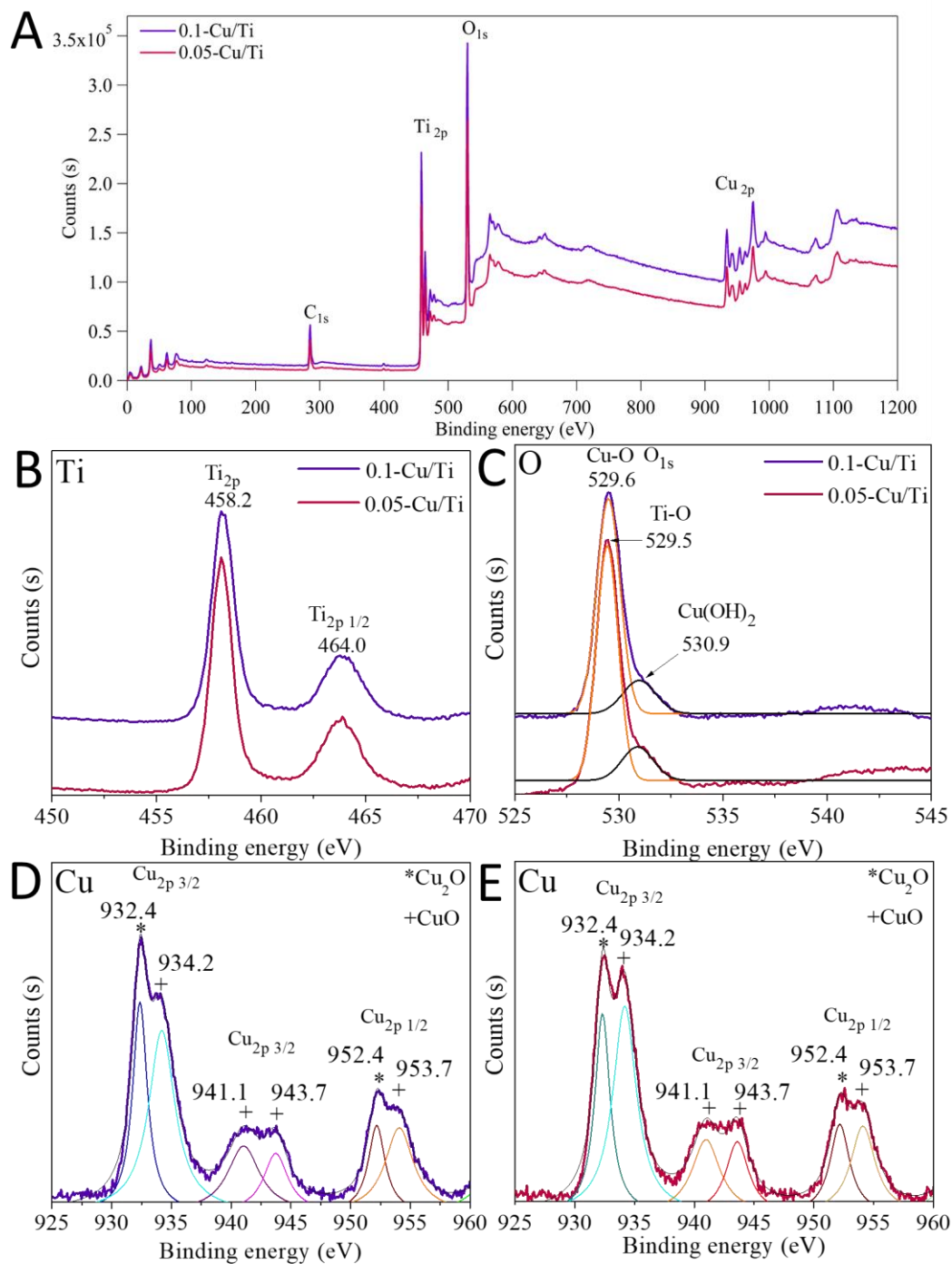


Figure 3. XPS spectra of the 0.1-Cu/Ti and 0.05-Cu/Ti composites A), titanium region B), oxygen region C), copper region of the 0.1-Cu/Ti composite D) and copper region of the 0.05-Cu/Ti composite E).

The Figure 4 displayed the UV-vis absorption spectra of Cu_xO particles, commercial P25 TiO_2 , and $\text{Cu}_x\text{O}/\text{TiO}_2$ composites. As expected, the absorption edge of the Cu_xO particles is located in the visible range, from 477 to 650 nm. In contrast, P25 TiO_2 possesses a well-defined UV absorption band starting from 325 to 410 nm. In the $\text{Cu}_x\text{O}/\text{TiO}_2$ composites, they clearly showed two bands, in the UV region and in the visible region, suggesting the potential adsorption in both, UV and visible spectra. In general, for all the composites, the first band started from 325-330 nm, while the ending of this band finished between 366 and 396 nm, in agreement to the copper oxides content, being the highest copper content sample (1-Cu/Ti) the lower value where the band was detected. On the other hand, the second band was observed around 477 nm in all the composites, and, the end of the band changed depending of the copper oxides content as in the first band, from 641 nm in the 1-Cu/Ti composite, to 606 nm in the 0.05-Cu/Ti composite. Furthermore, the intensity of this band decreased according to the weight ratio of the Cu_xO particles in the composites. The higher copper oxides content, the more intense absorption band. Therefore, these observations suggest that the copper oxides content influences the absorption edge of both, UV and visible bands. The band in UV part, red-shifted when the copper oxides content increases; meanwhile, in the visible region, the second band blue-shifted with the decrement of the copper species, whose intensity depends of the copper content.

In order to determine the E_g energy of the Cu_xO particles and the commercial P25 TiO_2 , Kubelka-Munk and Tauc methods were considered. The Kubelka-Munk function $F(R)$, (Equation 2), depends of experimental diffuse reflectance (R), and it is related to the absorption coefficient α and scattering coefficient S [23][24][25]. However, it is well-known that S is almost constant at any wavelength [24][26], therefore the $F(R)$ can be proportional to α , $F(R) \propto \alpha$ [26]. Additionally, it should be noted that, through the Tauc model, the absorption coefficient can be related to the band gap energy as shown the Equation 3 [27][28][29], where h is the Planck's constant, ν is the frequency of the wavelength of the

photon, A is a constant and n is related to the band gap transition in the material. Assuming the previous considerations, the experimental reflectance function can be associated to the band gap energy through the Equations 2 and 3, obtaining a function represented in the Equation 4. Thus, Tauc graph is obtained plotting $(F(R) * hv)^{\frac{1}{n}}$ versus the incident photon energy (hv) [30].

$$F(R) = \frac{(1-R)^2}{2*R} = \frac{\alpha}{S} \quad (2)$$

$$(\alpha * hv)^{\frac{1}{n}} = A(hv - E_g) \quad (3)$$

$$(F(R) * hv)^{\frac{1}{n}} = A(hv - E_g) \quad (4)$$

In this work, how Cu₂O is the predominant copper oxide phase, it was selected to calculate the band gap copper oxide particles, taking into account a direct allowed transition (n=1/2), reported previously [24][30][31]. However, both direct allowed and forbidden transitions were compared, and the E_g value was determined as 2.34 eV, almost the same in both cases (data not showed). The blue-shift of the band gap value respect to the E_g reported in the bulk Cu₂O (2.17 eV) [31] [32][33][34], can be explained by the polyhedral morphology of the particles, whose particular crystal facet structure determines its physical properties, as the optical behavior [33][35][36][37]. This phenomenon has been observed previously in similar Cu₂O particles [24][38]. Following the same procedure, indirect allowed transition (n=2) was selected to calculate E_g energy of the commercial P25 TiO₂ [38] [39], being the Y axis assigned as $(F(R)*hv)^{1/2}$. In this case, when F(R)=0, the calculated band gap is 3.31 eV. This value is in a good agreement with the previous literature reported [38][40].

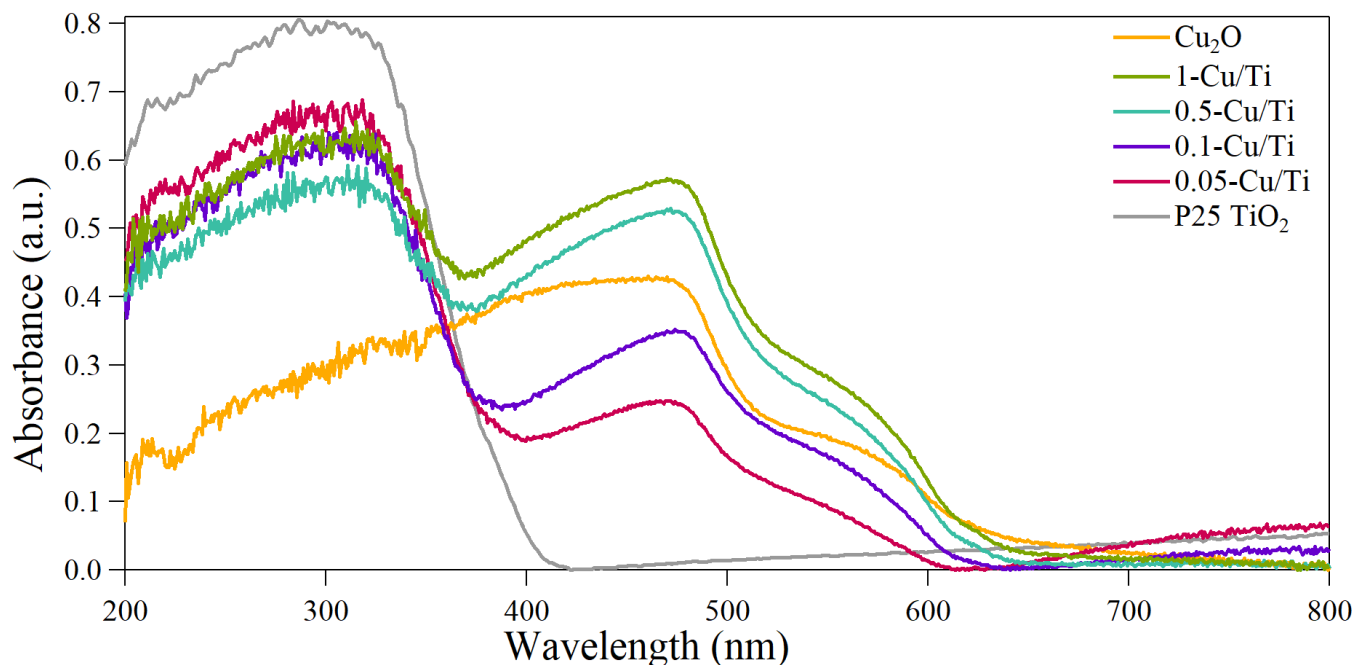


Figure 4. Optical absorption spectra of Cu_xO particles, commercial P25 TiO_2 and $\text{Cu}_x\text{O}/\text{TiO}_2$ composites.

The TRMC signals (microwave power variation $\frac{\Delta P}{P}(t)$) obtained upon laser irradiation for Cu_xO , P25 TiO_2 and the coupled $\text{Cu}_x\text{O}/\text{TiO}_2$ are displayed in the supporting information S1. This TRMC signal is assumed to rise from the high mobility electrons compared to positive holes. Thus, the signal intensity and decay pattern could be correlated to the photogenerated electrons at the surface of the photocatalysts. All the curves exhibit typical TRMC signal, corresponding to the production of charge carriers right after the laser excitation, followed by a decay, which is due to surface trapping, recombination and surface reaction [41].

After irradiation, the Cu_xO particles (Figure S1A) show an intense TRMC signal both, UV and visible range, enhancing in the visible range (520-580 nm), which it is in agreement with the spectral absorption

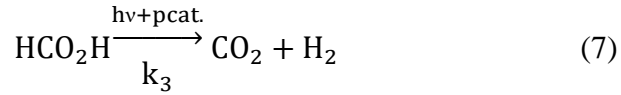
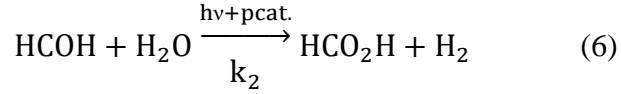
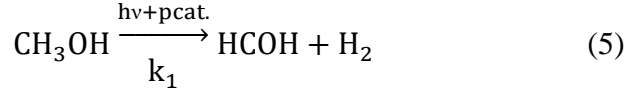
observed in DRS (Figure 4). In the same line, Figure S1B shows commercial P25 TiO₂ also produces photogenerated electrons under UV irradiation. However, the TRMC signal is observed to be weaker in the visible range than the UV range, where it was reached a high value. Indeed, the band gap of P25 TiO₂ was estimated to be around 3.31 eV, a slightly higher value than that of pure TiO₂ anatase phase [42], and absorbs only low fraction of the visible range. Coupling Cu_xO and P25 TiO₂ in the composites, extend the ability to produce charge carriers in the UV-visible range as suggested by the TRMC signal, where the signal produced under visible wavelengths (470 and 520 nm) is related to the Cu_xO proportion in these composites. In the sample 1-Cu/Ti, Figure S1C, the most intense signals were observed under wavelengths in the visible range, which is expected due to it has the highest Cu_xO weight ratio. However, the observed signal decays faster to low values, in all the wavelengths proved. Similarly, in the Figure S1D, the signals produced under visible range in the composite 0.5-Cu/Ti were sharper compared to the signal in the UV range (360 nm), and as in the previous composite, fast decay is observed in all the measurements. For the less-copper oxides composites, 0.1-Cu/Ti and 0.05-Cu/Ti, Figures S1E and F, the intensity of the maximum signal decreased respect to the high-copper oxides composites, in all the wavelengths tested. However, the decay stage was more stable, due to the intensity of the signal did not decrease at the same level observed in the high-copper oxides composites. In the composite 0.1-Cu/Ti, the generation of photoelectrons slightly decreased as a function of the wavelengths tested. The highest signal was detected under $\lambda=520$ nm, meanwhile the lowest it was observed when the material was irradiated at $\lambda=360$ nm. Nevertheless, the decay stage was not remarkable, and several signals were observed after the most intense peak, suggesting the probable generation of photoelectrons. Finally, for the 0.05-Cu/Ti composite, the best generation of photoelectrons was produced at $\lambda=470$ nm, respect to the other wavelengths (520 and 360 nm). Likely, the coupled effect between copper oxides and titanium dioxide, enhances the generation of photoelectrons at this wavelength.

3.6 Photocatalytic activity in batch processes

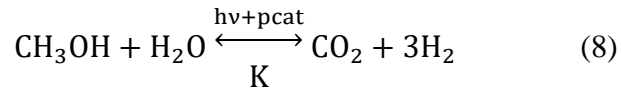
The photocatalytic behavior was performed into a conventional batch system. It is important to mention that, after the initial 30 min of irradiation, a notorious color change from slight yellow to deep purple was observed (Figure 5A), which was kept throughout the subsequent irradiation time. Surprisingly, when the irradiation was stopped, the solution of reaction came back to its original slight yellow color, after around 10 h. This phenomenon was observed in all the experiments, and it will be analyzed later.

The evolved H₂ and CO₂ gases were measured every hour and up to 8 h of irradiation time. As shown in Figure 5B, the Cu_xO polyhedral particles did not present photocatalytic activity throughout the evaluation period, due to the null H₂ production. For the commercial P25 TiO₂, low amount of H₂ was produced after 8 h under UV-vis irradiation. Conversely, the Cu_xO/TiO₂ composites showed significant H₂ generation, compared to each single oxide, being the less-copper oxide composites, 0.1-Cu/Ti and 0.05-Cu/Ti, the most active materials. Furthermore, their H₂ production rates increased almost eight times in these composites, compared to the H₂ production rate of commercial P25 TiO₂.

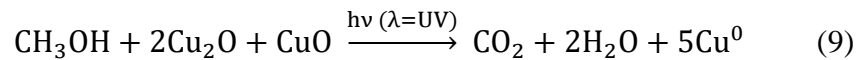
On the other hand, the CO₂ generation was measured to verify the stoichiometry of the methanol reforming reaction, and corroborated that, both H₂ and CO₂, could be consumed or produced in secondary reactions as water splitting reaction, in the H₂ production case. Figure 5C revealed that the composite materials produced higher CO₂, how in the H₂ generation case, respect to the single oxides. Furthermore, the CO₂ generation in the composites showed a similar tendency than the H₂ production, where the 0.1-Cu/Ti and 0.05-Cu/Ti composites produced the highest CO₂ amount. Note that, the CO₂ production rates with the 0.1-Cu/Ti and 0.05-Cu/Ti composites were fourteen times higher than the CO₂ production rate in commercial P25 TiO₂. According to the results presented in Table 3, the following set of reactions can occur to explain H₂ and CO₂ evolution:



With the overall reaction being;



where, $h\nu$ is the photon energy, pcat is the photocatalyst, k_x the equilibrium constant of each reaction and K is the global equilibrium constant. Therefore, in agreement with Equation 8, the H_2/CO_2 molar ratio must be 3. However, the average molar ratio of the experimental data showed different values for both, single oxides and the composites (Table 3). The H_2/CO_2 molar ratio calculated in the Cu_xO particles was 1.25, but, as the evolution of both gases was almost negligible, the photocatalytic activity is considered null. In contrast, the composites showed H_2/CO_2 molar ratios between 2.39 and 2.9, indicating a variation of the H_2 production or CO_2 generation, respect to the theoretical values expected, by a secondary reaction. Additionally, it is evident that this result has a relationship with the copper oxides weight ratio in each material, where the lower difference is observed in the 0.05-Cu/Ti composite. This result can be explained by the process represented in the following equation;



In this secondary process carried out under the irradiation time, methanol is oxidized to carbon dioxide and water, meanwhile both copper oxides (Cu_2O and CuO) are reduced to metallic copper (Cu^0) [43] [44]

[45] [46]. This reaction can be an additional way for the CO_2 generation, which can explain the H_2/CO_2 molar ratio lower than 3, the theoretical expected value. Additionally, there is a direct dependence with the copper oxides content and the process, and it should be the reason because the H_2/CO_2 molar ratio was lesser in the composites with the higher Cu_xO content, that in the composites with lower Cu_xO content. Thus, the process proposed in Equation 9 is favored in the composites with high copper oxides content, giving a lower H_2/CO_2 molar ratio. In fact, this reaction explains the change of color of the solution during the irradiation time as well. When the composites are irradiated, the process represented in the Equation 9 takes place, and the copper oxides in the composites are reduced to metallic copper, changing the color of the solution from slight yellow, characteristic color of copper oxides, to deep purple. After, when the irradiation is stopped, the oxidation environment and the presence of TiO_2 promotes the re-oxidation of the metallic copper, as it is explained in the discussion section.

On the other hand, in commercial P25 TiO_2 , the H_2/CO_2 molar ratio was almost the double respect to the theoretical value, around 5.48. In this case, the increment of molar ratio is due to the increment of the H_2 production, respect to the expected stoichiometric amount from the methanol photoreforming. Therefore, the P25 TiO_2 is able to carry out methanol photoreforming reaction [47] [48] [49], and the additional H_2 amount can be produced by water splitting, which has been reported for this material previously [50] [51].

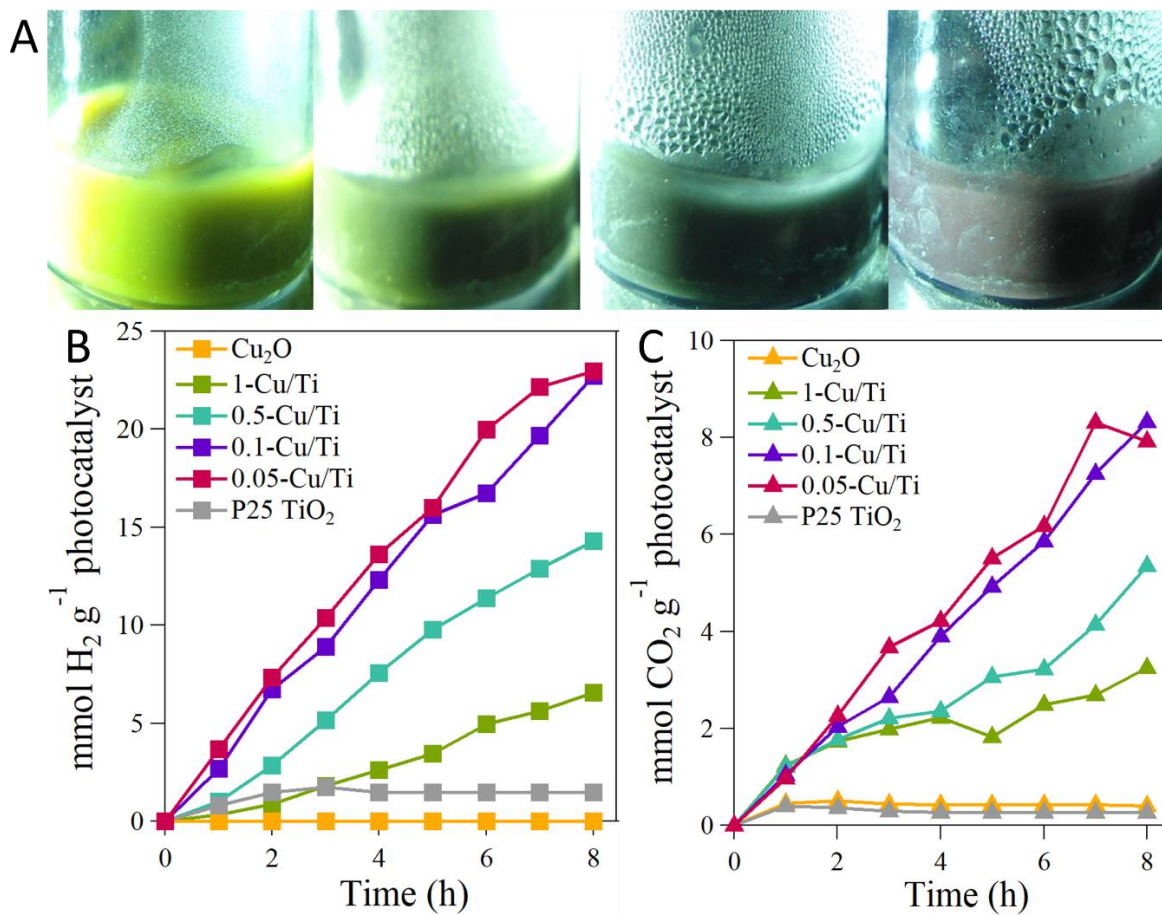


Figure 5. Color change of the solution of reaction after of 30 minutes of irradiation, and during the photocatalytic process A), H₂ production B) and CO₂ evolution C) by methanol photoreforming under solar simulator at 150 W, with a concentration of 1 g L⁻¹ of photocatalyst.

Table 3. H₂ and CO₂ evolution

Photocatalyst	H ₂ mmol g ⁻¹	H ₂ evolution rate mmol g ⁻¹ h ⁻¹	CO ₂ mmol g ⁻¹	CO ₂ evolution rate mmol g ⁻¹ h ⁻¹	Molar ratio H ₂ /CO ₂
Cu _x O	0.05	0.007	0.04	0.01	1.25
1-Cu/Ti	6.21	0.69	2.59	0.29	2.39
0.5-Cu/Ti	14.29	1.79	5.34	0.67	2.67
0.1-Cu/Ti	22.72	2.84	8.32	1.04	2.73
0.05-Cu/Ti	22.94	2.86	7.91	0.99	2.90
Commercial P25 TiO ₂	1.48	0.37	0.27	0.07	5.48

For comparison purposes, the evaluation of 0.1-Cu/Ti composite was performed in the water splitting reaction, and the results are displayed in Figure 6A. Notoriously, no H₂ evolution was detected in this reaction (water + composite + irradiation), which means that, methanol photoreforming is the reaction carried out for H₂ production. Methanol is a hole collector and could inject electrons in the CB of the Cu_xO/TiO₂ composite [52]. This dissociative adsorption of methanol is followed by the release of the hydrogen radicals. Thus, the produced hydrogen comes from the released protons after methanol photooxidation, following the Equations 5-7. Furthermore, it is important to mention that, no color change was observed during water splitting evaluation, confirming the additional CO₂ generation process depicted in the Equation 9, where methanol is involved.

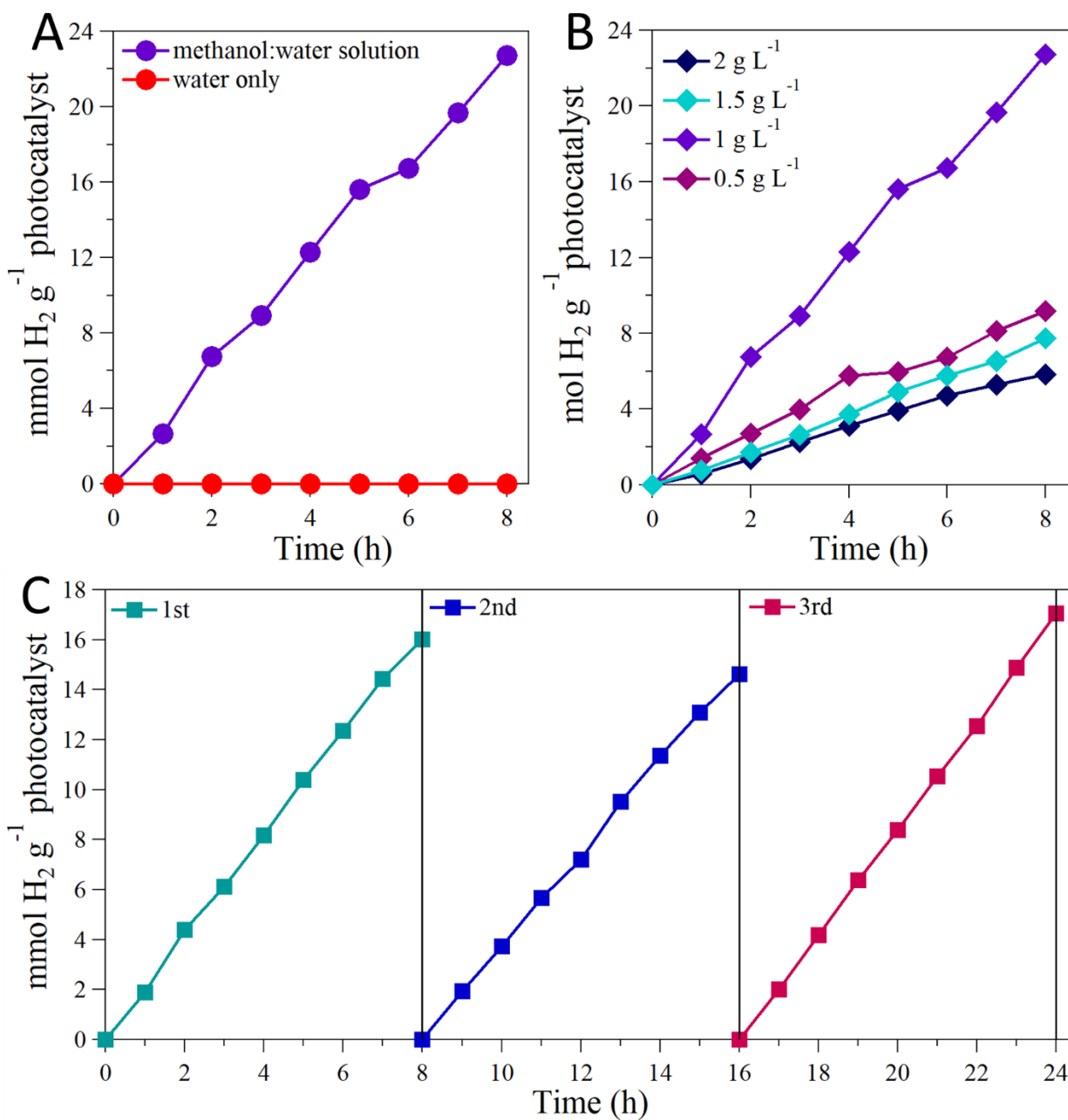


Figure 6. Methanol photoreforming vs water splitting processes A), effect of the photocatalyst concentration B), and the reaction cycles C) in H₂ evolution for the 0.1-Cu/Ti composite.

Additionally, the photocatalyst concentration effect was studied with the same composite (0.1-Cu/Ti), using concentrations from 0.5 g L⁻¹ to 2 g L⁻¹ (Figure 6B). Clearly, methanol photoreforming is highly sensitive at the catalyst concentration, since the best photocatalytic performance was reached by using a 1 g L⁻¹ catalyst concentration. Indeed, at low catalyst concentration (i.e. 0.5 g L⁻¹), not enough proton conversion sites are available to be converted into molecular hydrogen. On the contrary, by increasing the catalyst load (1.5-2 g L⁻¹), a significant decrease of the H₂ production rate is observed, which is attributed to light scattering of the material hindering the illumination in the reaction system, as well as agglomeration-sedimentation of the photocatalyst, despite of the stirring of the solution of reaction [53] [54] [55] [56].

Finally, in the Figure 6C, the cyclic capacity results of the 0.1-Cu/Ti composite are presented. The photoactivity of the material was kept after three reaction cycles, being the maximum H₂ production on each cycle between 15 and 17 mmol of H₂ per gram of photocatalyst. This significative stability, despite of aqueous environment and irradiation for at least 24 hours, demonstrated that the Cu_xO/TiO₂ composites are good candidates to reuse more than once for methanol photoreforming, without to lose its photocatalytic performance. Furthermore, it is important to point out that, the slight yellow color of the composite changed to deep purple on each reaction cycle, and then, after stopping the irradiation, washing and drying it, its color came back to slight yellow as in the beginning of the reaction, before the irradiation.

Thus, as a brief, the photoactivity was strongly susceptible to the Cu_xO amount in the composites, obtaining the best results at low Cu_xO concentrations (i.e., 0.1-Cu/Ti and 0.05-Cu/Ti composites). Then, an excess of the optimal amount of Cu_xO can promote the recombination of the photo charge carriers, decreasing the photoactivity [11][18][57][58], moreover the feasibility of the secondary oxidation process of methanol, where CO₂ and H₂O instead of H₂ are produced.

X-ray photoelectron spectroscopy after irradiation

To identify the copper species formed after irradiation, XPS characterization of 0.1-Cu/Ti composite was performed at the end of methanol photoreforming process (Figure 7). The deep purple color of the material after the evaluation was keeping partially for the XPS analysis. Specifically, oxygen and copper regions were analyzed, and the same regions of the initial spectra of the composite before evaluation were added as a comparison. As it is shown in the plots, the intensity of the signals after the evaluation decreased respect to the signal observed in the pristine sample. In Figure 7A, the O 1s spectra show a peak at 529.6 eV, attributed to CuO, and a shoulder at 530.9 eV, that it was mentioned to correspond to the presence of Cu(OH)₂ in the pristine samples. After irradiation, the signal at 529.6 eV was found as well, and additional shoulder appeared at 531.3 eV, which was associated at the presence of no-stoichiometric titanium dioxide (TiO_{1.55} or TiO_{1.35}). For the Cu 2p region (Figure 7B), the peaks localized at 932.5 and 952.4 eV, referred to Cu₂O, correspond to Cu 2p_{3/2} and Cu 2p_{1/2}, respectively. Additionally, the presence of CuO was confirmed by the peaks at 934.4 and 954.3 eV, assigned as Cu 2p_{3/2} and Cu 2p_{1/2}, along with the satellite peaks at 941.4 and 943.7 eV, observed in both spectra. No additional peaks were found in this region, so that, no clear evidence about the metallic copper presence after the evaluation.

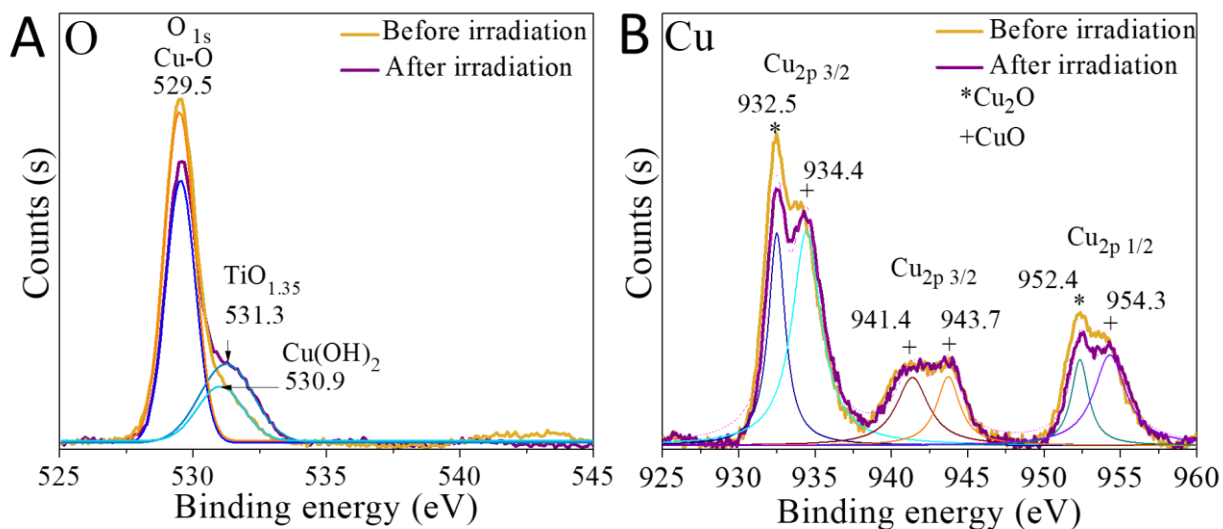


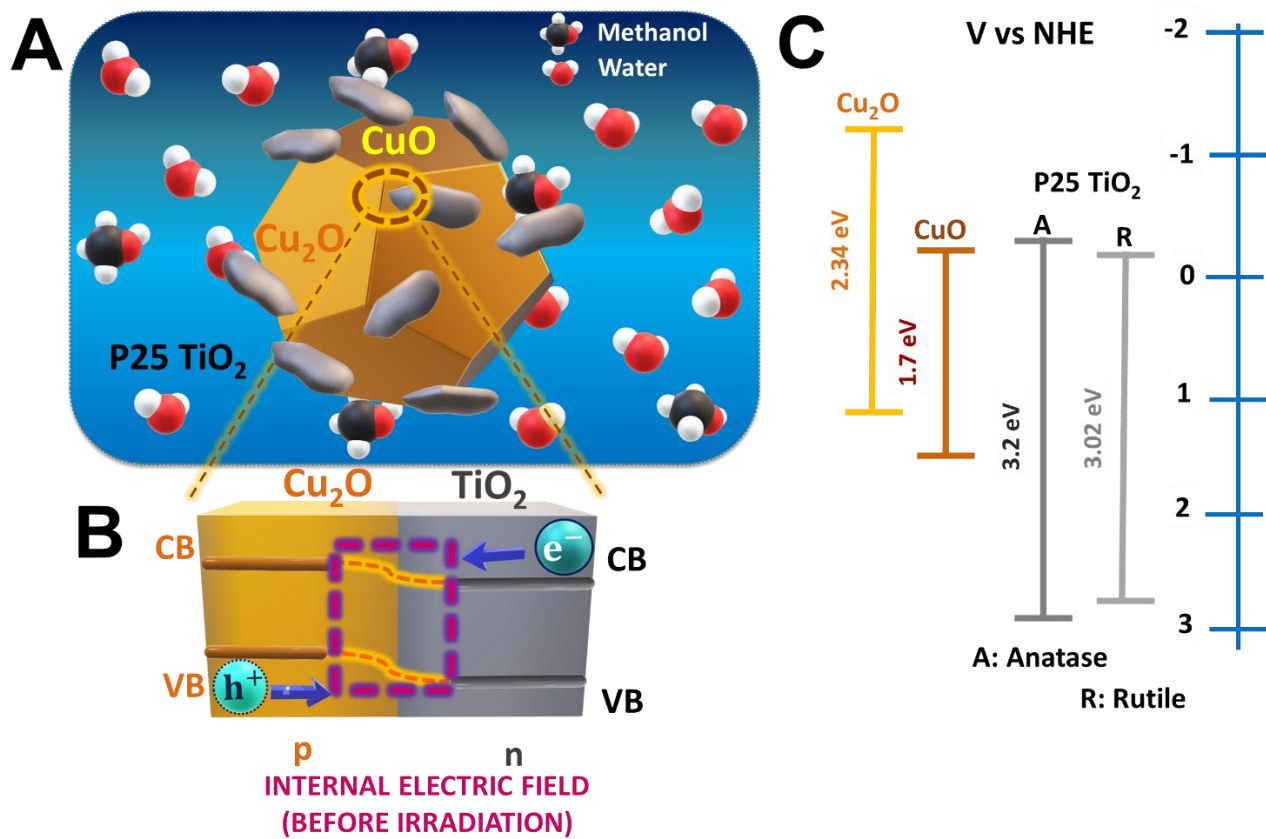
Figure 7. XPS spectra of the 0.1-Cu/Ti composite in oxygen A), and copper B) regions, before and after irradiation.

4. Discussion

From a global point of view, methanol photoreforming was fundamentally influenced by the spatial distribution, composition and electronic properties of the $\text{Cu}_x\text{O}/\text{TiO}_2$ composites. According to XRD data and SEM micrographs showed in Figures 1 and 2, both Cu_xO and TiO_2 particles coexists as separated phases. However, they have close contact with each other randomly, without any specific configuration. Due to this spatial distribution, both Cu_xO and TiO_2 particles are in direct contact with the aqueous methanol solution. Therefore, during irradiation, the photogenerated charge carriers of both semiconductors can participate in redox reactions on the surface, since there is a high probability of charge transfer between the semiconductor-liquid interface, as it is illustrated in the Scheme 1A [11]. In fact, also, it is important to highlight the existence of four species in the composites, and consider their contribution in the electronic properties of the whole system. The first specie is Cu_2O , as polyhedral particles, identified by several techniques such as XRD, SEM and XPS. Furthermore, in the same particles, CuO was detected

by XRD patterns and it was corroborated in the 0.1-Cu/Ti and 0.05-Cu/Ti samples via XPS spectra, being part of the composites as well. Likely, this specie (CuO) can be presented over the surface oxidation of Cu₂O particles, forming of a thin layer over the particles, as it has been reported elsewhere [32][59][60][61]. The third and fourth components are the crystalline phases in commercial P25 TiO₂, anatase and rutile, whose standard proportion has been defined as 80:20 [11][62]. These phases were corroborated by XRD patterns in all composites.

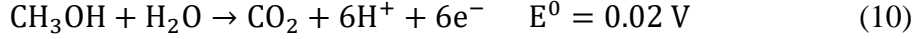
After the description of the presented species in the composites, it is important to consider the type of interactions between them. The most important interaction is resulted of the coexistence between Cu₂O and TiO₂, called p-n heterojunction, due to the nature of both semiconductors [63]. In the interface of the semiconductors, and before the irradiation, the electrons from TiO₂, n-type semiconductor, migrate toward p-type semiconductor, Cu₂O. At the same time, holes from this p-type semiconductor travel to the opposite side to n-type semiconductor, due to the difference of the Fermi levels of the two oxides. Thus, when the charge equilibrium is reached by the difference of their Fermi levels, an internal electric field is created [64], as it can see in the Scheme 1B.



Scheme 1. Structure and proposed band alignment of the $\text{Cu}_x\text{O}/\text{TiO}_2$ composites.

Under these premises, the spatial distribution of the particles and the existence of four species in the composites, it was proposed a band alignment in the photocatalysts, through the E_g energy and their band edge commonly reported (Scheme 1C). According to the diffuse reflectance spectrum and Tauc plot shown in Figure 4, the Cu_2O band gap was calculated as 2.34 eV, slightly higher than the most common value reported in the literature, around 2-2.2 eV [14] [65] [66]. Despite of the increment in the E_g in the synthesized sample, the valence band (VB) and conduction band (CB) position, reported at 1.07 and -1.13 V [42] [67] respectively, are considered in the alignment proposed. In the case of CuO, even though its band gap was not determined experimentally, its E_g alignment was taken into account in the composites (the VB and CB positions as 1.5 and -0.2 V respect to NHE, respectively, [67] [68] [69]), due to it is part

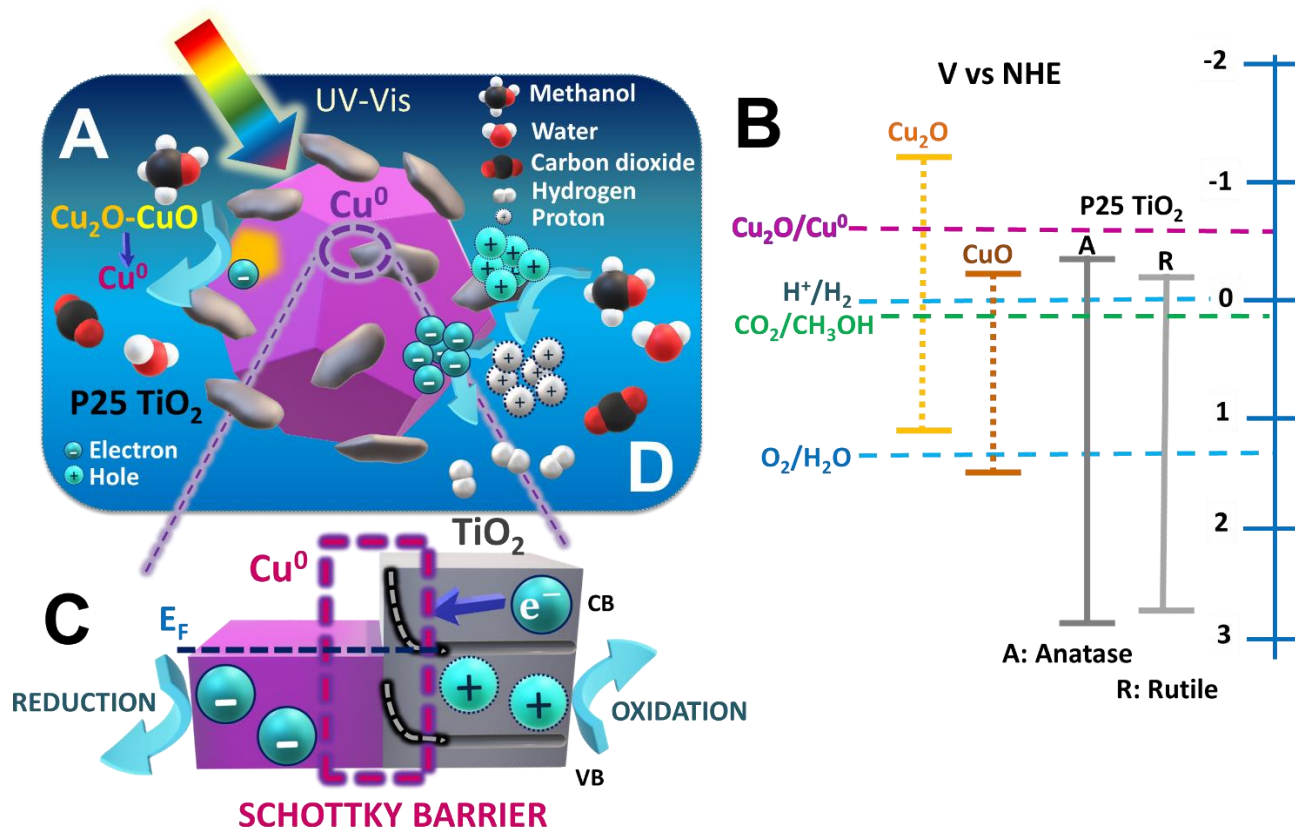
of the Cu_2O particles and can contribute in the electronic properties of the composites. Concerning to the commercial P25 TiO_2 , the E_g was estimated as 3.31 eV. Now, it should be take into account that, this value is composed by the E_g of pure anatase (3.2 eV) and pure rutile (3.02 eV) [11] [70]. In anatase phase, the positions of the VB and CB have been measured around 2.9 and -0.29 V respect to NHE [67], meanwhile for rutile phase, the E_g position has been identified underneath respect to anatase CB and VB [64]. Thus, the proposed E_g position of each component in the composite are represented following these assumptions. Accordingly, a reaction path can be proposed starting from the irradiation of the composites with a simulated solar light. The UV wavelength excites the P25 TiO_2 particles, meanwhile the visible light excites copper oxides (Cu_2O , CuO), where the generation of electron-hole pair in the semiconductors happens. The photogenerated charge carriers can migrate from each semiconductor to the solid-liquid interphase directly, by the spatial distribution of the particles, as well as to the $\text{Cu}_x\text{O-TiO}_2$ contact. In the last case, as an internal electric field was formed in the p-n heterojunction, the electrons migrate from Cu_xO to the TiO_2 CB, first to anatase phase and after that to rutile phase, where it is possible an accumulation of the charge carriers [71]. At the same time, the photogenerated holes can remain in the Cu_2O and CuO VB, while, the generated holes in the VB of P25 TiO_2 migrate toward the Cu_2O VB, by the proposed band alignment, driving a spatial separation of the charge carriers through the composite. Thus, the overall scheme of photoredox reactions leads to minimal charge recombination, supported by semiconductor thermodynamics [18], [64], [72]–[74]. Additionally, aqueous methanol plays an active role as hole scavenger at this stage, avoiding the charge recombination and donating protons and electrons required for the H_2 production [48] [75]. The general reaction was showed in the evaluation section (Equation 8), and it can rewrote as the Equation 10. In agreement of this Equation, the theoretical oxidation potential required is 0.02 V [76].



Additionally, methanol could be able to reduce copper species, following the secondary reaction (Equation 9) proposed in the evaluation section. Initially, the photocatalyst-aqueous methanol solution presented a slight yellow color, due to the $\text{Cu}_x\text{O-TiO}_2$ composites. After irradiation, the color of the solution changed progressively toward intense red-purple (Figure 6A). This deep red-purple color in copper species has been attributed to the existence of metallic copper (Cu^0) [77]–[79]. In order to prove this assumption, the 0.1-Cu/Ti sample was analyzed by XPS after irradiation (Figure 8), but any clear evidence was found about the Cu^0 presence. However, the color change of the photocatalyst-aqueous methanol system, the increment of CO_2 evolution calculated through the H_2/CO_2 molar ratio in the experimental results, and null color change during water splitting test, can support this assumption.

Besides, the change in the oxidation state is feasible at the band alignment proposed. The potential required to reduce Cu_2O to Cu^0 is -0.360 V [80], which is located inside of the band gap of the Cu_2O . Therefore, an intense radiation over Cu_2O particles can promote their self-reduction to Cu^0 , by the photogenerated electrons [81], further to the secondary oxidation of methanol proposed. Additionally, it should consider that the high flux of the charge carriers in the p-n heterojunction can increase the electron density in the P25 TiO_2 CB [73], whose position is near at the potential required to form Cu^0 as well. Thereby, the combined effect of the secondary methanol oxidation described and the electrons from VB of Cu_2O or even in the p-n heterojunction can reduce copper species from Cu^{+2} and Cu^{+1} to Cu^0 [46], which represented in the Scheme 2A. Thus, the $\text{Cu}^0/\text{P25 TiO}_2$ system is proposed after irradiation of the evaluation medium, and the required reduction potential for this process is represented in the optical band alignment of the initial species (Scheme 2B).

The presence of the Cu^0 particles modifies the charge transfer mechanism in the composites. After the copper reduction process, a Schottky barrier is formed between Cu^0 and P25 TiO_2 (Scheme 2C). This Schottky barrier is able to trap electrons, which decrease the recombination rate of the photocarriers. Therefore, the electron transfer carries out from P25 TiO_2 to Cu^0 particles, due to the work function in the metal is higher than the semiconductor one. This electron migration continues until to reach the equilibrium, where the Fermi levels of Cu^0 , as well as P25 TiO_2 are aligned with CB of P25 TiO_2 . By this way, P25 TiO_2 and Cu^0 particles gain an excess of positive and negative charges, respectively [11] [82]. The excess of negative charge in the Cu^0 particles, added to the efficient charge carries separation, promote the H^+ reduction, enhancing the H_2 production, according with the equation 10 (Scheme 2D).



Scheme 2. Photocatalytic performance of the $\text{Cu}_x\text{O}/\text{TiO}_2$ composites during irradiation.

Additionally to the process previously described, the existence of the Cu₂O/CuO hybrid structure in the composites represents a double way to generate electrons [73] [83] and, the homojunction between anatase-rutile improves the charge separation [11] [73] [84] [85]. Several hours after turning off the irradiation, the composites returned to the initial slight yellow from the red-purple color, indicating the oxidation state change from Cu⁰ to copper oxides again. The next reactions shows the likely path of the Cu⁰ oxidation to the Cu₂O particles during the photocatalytic test and after irradiation, where P25 TiO₂ participates [81]:



Remaining holes from P25 TiO₂ participate actively in the re-oxidation of Cu⁰ to Cu_xO, playing a critical role in the copper re-oxidation process after irradiation. Finally, a comparative table was performed between previous reports and the obtained results in the current work (Table S1). The system copper species-titanium dioxide has been widely studied, due to the significative performance of the combination of these species during the photocatalytic hydrogen production through alcohols reforming. Among the strategies used, have been reported the modification of the copper oxides morphology, size, and the ratio respect to titanium dioxide. For the last one, commercial P25 TiO₂ has been selected as a titanium source, although several groups have synthesized it, modifying its morphology and size. Also, different elements as silver have been added to this kind of systems. Besides, a variety of sacrificial agents have been used for the alcohols reforming, although, in the most of the cases, methanol has shown the best results. Respect to the source light, the works reported a potency between 100 to 500 W, with high- energy wavelengths in the UV region. The maximum H₂ production rate of each case is mainly linked to the alcohol proportion in the reaction medium and the structural properties of the oxides. The obtained values are in the range

from 0.009 to 286 mmol g⁻¹ h⁻¹, however, the most of them are between 2.048 and 4.5 mmol g⁻¹ h⁻¹. The best H₂ production rate of this work is in this range, being 2.86 g⁻¹ h⁻¹. This result could be considered exceptional, taking into account the easy synthesis method selected, low copper oxide ratio respect to P25 TiO₂ (0.01,0.05 to1), methanol proportion used (1:10) and the low power of the irradiation source (150 W), due to that similar or slightly higher results have been reported under difficult synthesis methods, higher alcohol proportion and potency of irradiation source.

4. Conclusions

The Cu_xO/TiO₂ composites with different weight ratios were synthesized successfully by a simple, room temperature wet-mixed method, where synthesized-copper particles, composed by Cu₂O and CuO, and the commercial P25 TiO₂ were used as precursors. Through this method, the composites acquire specific spatial distribution, where both particles are in contact with the solution of reaction, being a convenient distribution to participate in the redox reactions. Besides, the composites exhibited two broad optical absorption bands, from visible to UV regions, demonstrating photoactivity under both spectral regions. This assumption was corroborated through TRMC measurements, where the irradiation with different wavelengths showed a direct relationship between the amount of photocarriers produced, the dominant specie, and the wavelength used; more P25 TiO₂ more photocarriers under UV light, more Cu_xO oxides, more photocarriers under visible light. The as-synthesized composites were evaluated in methanol photoreforming reaction, by batch system. During irradiation, the Cu₂O/CuO species in the composites undergo a self-reduction to Cu⁰, which was verified by a change of color of the photocatalyst-aqueous methanol solution, from slight yellow to intense red-purple. This behavior was attributed of different reasons. Firstly, the secondary oxidation reaction of methanol, corroborated by the decrease of H₂/CO₂ molar ratio during the evaluation, where the copper oxides participate being reduced to metallic copper; and secondly, the efficient spatial separation of the charge carries due to the formation of p-n

heterojunction, which leads the reduction of copper oxides to metallic copper, by high electron density. In consequence, a Schottky barrier was created in the new Cu⁰/P25 TiO₂ composite, resulting in high density of negative charges, which enhances the H₂ production, by the protons availability in the aqueous reaction medium and the increment of the stability of the photocatalyst. Thus, the charge carriers are able to participate in the photocatalytic reactions and modify the photocatalyst itself. The importance of methanol was proved during water splitting test, where the null H₂ production and no change of color were observed. Furthermore, the Cu_xO content influences the photocatalytic performance, where the number of active sites and light scattering-sedimentation phenomena play a critical role. Therefore, the combination of spatial distribution, the key role of methanol presence, the p-n heterojunction, the Cu_xO/TiO₂ weight ratio, the presence of four species, and P25 TiO₂ homojunction allow to self-improve the photocatalysts and to enhance the photoactivity towards H₂ production via methanol photoreforming.

Acknowledgements

The authors acknowledge the financial supports of SIP-20180100 and SIP-20180893 projects. FPH is grateful for CONACyT and BEIFI fellowships. M.V. acknowledges Université Paris-Saclay for the financial support through the Chaire Jean d'Alembert program and the IRS MOMENTOM (Initiative de Recherche Stratégique).

References

- [1] J. O. Abe, A. P. I. Popoola, E. Ajenifuja, and O. M. Popoola, "Hydrogen energy, economy and storage: Review and recommendation," *International Journal of Hydrogen Energy*, vol. 44, no. 29. Elsevier Ltd, pp. 15072–15086, 07-Jun-2019.
- [2] S. E. Hosseini and M. A. Wahid, "Hydrogen production from renewable and sustainable energy resources: Promising green energy carrier for clean development," *Renew. Sustain. Energy Rev.*, vol. 57, pp. 850–866, 2016.

- [3] P. Nikolaidis and A. Poulikkas, “A comparative overview of hydrogen production processes,” *Renew. Sustain. Energy Rev.*, vol. 67, pp. 597–611, 2017.
- [4] S. Wang *et al.*, “Controllable sonochemical synthesis of $\text{Cu}_2\text{O}/\text{Cu}_2(\text{OH})_3\text{NO}_3$ composites toward synergy of adsorption and photocatalysis,” *Appl. Catal. B Environ.*, vol. 164, no. 3, pp. 234–240, 2015.
- [5] M. E. El-Khouly, E. El-Mohsnawy, and S. Fukuzumi, “Solar energy conversion: From natural to artificial photosynthesis,” *J. Photochem. Photobiol. C Photochem. Rev.*, vol. 31, pp. 36–83, 2017.
- [6] K. C. Christoforidis and P. Fornasiero, “Photocatalytic Hydrogen Production: A Rift into the Future Energy Supply,” *ChemCatChem*, vol. 9, no. 9, pp. 1523–1544, 2017.
- [7] M. Jung, J. N. Hart, D. Boensch, J. Scott, Y. H. Ng, and R. Amal, “Hydrogen evolution via glycerol photoreforming over Cu-Pt nanoalloys on TiO_2 ,” *Appl. Catal. A Gen.*, vol. 518, pp. 221–230, 2016.
- [8] G. Colón, “Towards the hydrogen production by photocatalysis,” *Appl. Catal. A Gen.*, vol. 518, no. December 2015, pp. 48–59, 2016.
- [9] M. Ge *et al.*, “A review of TiO_2 nanostructured catalysts for sustainable H_2 generation,” *Int. J. Hydrogen Energy*, vol. 42, no. 12, pp. 8418–8449, 2017.
- [10] N. S. Ibrahim, W. L. Leaw, D. Mohamad, S. H. Alias, and H. Nur, “A critical review of metal-doped TiO_2 and its structure–physical properties–photocatalytic activity relationship in hydrogen production,” *Int. J. Hydrogen Energy*, vol. 45, no. 53, pp. 28553–28565, Oct. 2020.
- [11] L. Clarizia, D. Russo, I. Di Somma, R. Andreozzi, and R. Marotta, “Hydrogen generation through solar photocatalytic processes: A review of the configuration and the properties of effective metal-based semiconductor nanomaterials,” *Energies*, vol. 10, no. 10, 2017.
- [12] L. Li, L. Xu, W. Shi, and J. Guan, “Facile preparation and size-dependent photocatalytic activity

- of Cu₂O nanocrystals modified titania for hydrogen evolution,” *Int. J. Hydrogen Energy*, vol. 38, no. 2, pp. 816–822, Jan. 2013.
- [13] M. R. Pai *et al.*, “Solar Energy Materials & Solar Cells A comprehensive study on sunlight driven photocatalytic hydrogen generation using low cost nanocrystalline Cu-Ti oxides,” *Sol. Energy Mater. Sol. Cells*, vol. 154, pp. 104–120, 2016.
- [14] L. Liu, W. Yang, W. Sun, Q. Li, and J. K. Shang, “Creation of Cu₂O@TiO₂ composite photocatalysts with p - N heterojunctions formed on exposed Cu₂O facets, their energy band alignment study, and their enhanced photocatalytic activity under illumination with visible light,” *ACS Appl. Mater. Interfaces*, vol. 7, no. 3, pp. 1465–1476, 2015.
- [15] Z. Geng *et al.*, “Incorporation of Cu₂O nanocrystals into TiO₂ photonic crystal for enhanced UV–visible light driven photocatalysis,” *J. Alloys Compd.*, vol. 644, pp. 734–741, 2015.
- [16] J. Low, J. Yu, M. Jaroniec, S. Wageh, and A. A. Al-Ghamdi, “Heterojunction Photocatalysts,” *Adv. Mater.*, vol. 29, no. 20, p. 1601694, May 2017.
- [17] Y. Liu *et al.*, “TiO₂/Cu₂O Core/Ultrathin Shell Nanorods as Efficient and Stable Photocatalysts for Water Reduction,” *Angew. Chemie - Int. Ed.*, vol. 54, no. 50, pp. 15260–15265, 2015.
- [18] Y. Li, B. Wang, S. Liu, X. Duan, and Z. Hu, “Synthesis and characterization of Cu₂O/TiO₂ photocatalysts for H₂ evolution from aqueous solution with different scavengers,” *Appl. Surf. Sci.*, vol. 324, pp. 736–744, 2015.
- [19] L. Buzzetti, G. E. M. Crisenza, and P. Melchiorre, “Mechanistic Studies in Photocatalysis,” *Angew. Chemie - Int. Ed.*, vol. 58, no. 12, pp. 3730–3747, 2019.
- [20] K. P. Sundar and S. Kanmani, “Progression of Photocatalytic reactors and it’s comparison: A Review,” *Chemical Engineering Research and Design*, vol. 154. Institution of Chemical Engineers, pp. 135–150, 01-Feb-2020.

- [21] D. Jiang, C. Xing, X. Liang, L. Shao, and M. Chen, "Synthesis of cuprous oxide with morphological evolution from truncated octahedral to spherical structures and their size and shape-dependent photocatalytic activities," *J. Colloid Interface Sci.*, vol. 461, pp. 25–31, 2016.
- [22] M. N. Ghazzal, O. Deparis, J. De Coninck, and E. M. Gaigneaux, "Tailored refractive index of inorganic mesoporous mixed-oxide Bragg stacks with bio-inspired hygrochromic optical properties," *J. Mater. Chem. C*, vol. 1, no. 39, pp. 6202–6209, 2013.
- [23] P. Apopei, C. Catrinescu, C. Teodosiu, and S. Royer, "Mixed-phase TiO₂ photocatalysts: Crystalline phase isolation and reconstruction, characterization and photocatalytic activity in the oxidation of 4-chlorophenol from aqueous effluents," *Appl. Catal. B Environ.*, vol. 160–161, no. 1, pp. 374–382, 2014.
- [24] D. Gupta, S. R. Meher, N. Illyaskutty, and Z. C. Alex, "Facile synthesis of Cu₂O and CuO nanoparticles and study of their structural, optical and electronic properties," *J. Alloys Compd.*, vol. 743, pp. 737–745, 2018.
- [25] P. K. Sharma, M. A. L. R. M. Cortes, J. W. J. Hamilton, Y. Han, J. A. Byrne, and M. Nolan, "Surface modification of TiO₂ with copper clusters for band gap narrowing," *Catal. Today*, vol. 321–322, no. July 2017, pp. 9–17, 2019.
- [26] U. Pal, "Use of diffuse reflectance spectroscopy for optical characterization of un-supported nanostructures," *Rev. Mex. Física*, vol. 53, no. 5, pp. 18–22, 2007.
- [27] O. Messaoudi *et al.*, "Correlation between optical and structural properties of copper oxide electrodeposited on ITO glass," *J. Alloys Compd.*, vol. 611, pp. 142–148, 2014.
- [28] H. Lahmar, F. Setifi, A. Azizi, G. Schmerber, and A. Dinia, "On the electrochemical synthesis and characterization of p-Cu₂O/n-ZnO heterojunction," *J. Alloys Compd.*, vol. 718, pp. 36–45, 2017.

- [29] M. K. Hossain *et al.*, “A comparative study on the influence of pure anatase and Degussa-P25 TiO₂ nanomaterials on the structural and optical properties of dye sensitized solar cell (DSSC) photoanode,” *Optik (Stuttg.)*, vol. 171, no. May, pp. 507–516, 2018.
- [30] D. Nunes *et al.*, “Room Temperature Synthesis of Cu₂O Nanospheres: Optical Properties and Thermal Behavior,” *Microsc. Microanal.*, vol. 21, no. 1, pp. 108–119, 2015.
- [31] H. Amekura and N. Kishimoto, “Fabrication of Oxide Nanoparticles by Ion Implantation and Thermal Oxidation,” *Towar. Funct. Nanomater.*, pp. 1–75, 2009.
- [32] M. Leng *et al.*, “Polyhedral 50-Facet Cu₂O Microcrystals Partially Enclosed by {311} High-Index Planes: Synthesis and Enhanced Catalytic CO Oxidation Activity,” *J. Am. Chem. Soc.*, vol. 132, no. 48, pp. 17084–17087, Dec. 2010.
- [33] S. Sun and Z. Yang, “Recent advances in tuning crystal facets of polyhedral cuprous oxide architectures,” *RSC Adv.*, vol. 4, no. 8, pp. 3804–3822, 2014.
- [34] I. V. Bagal *et al.*, “Cu₂O as an emerging photocathode for solar water splitting - A status review,” *Int. J. Hydrogen Energy*, vol. 44, no. 39, pp. 21351–21378, 2019.
- [35] M. Yang and J. J. Zhu, “Spherical hollow assembly composed of Cu₂O nanoparticles,” *J. Cryst. Growth*, vol. 256, no. 1–2, pp. 134–138, 2003.
- [36] D. Sai Cong, “Synthesis and Optical Properties of Cu₂O and Au-Cu₂O core-shell particles,” *VNU J. Sci. Math. - Phys.*, vol. 33, no. 4, pp. 73–79, 2017.
- [37] J. Ouyang, H. Yang, and A. Tang, “Shape controlled synthesis and optical properties of Cu₂O micro-spheres and octahedrons,” *Mater. Des.*, vol. 92, pp. 261–267, 2016.
- [38] D. Nagy, C. Chao, B. Marzec, F. Nudelman, M. C. Ferrari, and X. Fan, “Effect of Ag Co-catalyst on TiO₂-Cu₂O nanocomposites structure and apparent visible photocatalytic activity,” *J. Environ. Manage.*, vol. 260, no. November 2019, 2020.

- [39] X. Guo *et al.*, “Photocatalytic properties of P25-doped TiO₂ composite film synthesized via sol-gel method on cement substrate,” *J. Environ. Sci. (China)*, vol. 66, pp. 71–80, 2018.
- [40] S. S, K. L. Nagashree, T. Maiyalagan, and G. Keerthiga, “Photocatalytic degradation of 2,4-dichlorophenoxyacetic acid - A comparative study in hydrothermal TiO₂ and commercial TiO₂,” *Appl. Surf. Sci.*, vol. 449, pp. 371–379, 2018.
- [41] C. Colbeau-Justin, M. Kunst, and D. Huguenin, “Structural influence on charge-carrier lifetimes in TiO₂ powders studied by microwave absorption,” *J. Mater. Sci.*, vol. 38, no. 11, pp. 2429–2437, Jun. 2003.
- [42] C. Jiang, A. Savio, J. A. Moniz, A. Wang, T. Zhang, and J. Tang, “Photoelectrochemical devices for solar water splitting – materials and challenges,” *Chem. Soc. Rev. Chem. Soc. Rev*, vol. 46, no. 46, pp. 4645–4660, 2017.
- [43] T. H. Fleisch and G. J. Mains, “Reduction of copper oxides by UV radiation and atomic hydrogen studied by XPS,” *Appl. Surf. Sci.*, vol. 10, no. 1, pp. 51–62, Jan. 1982.
- [44] D. Luo *et al.*, “Cu⁽⁰⁾/TiO₂ composite byproduct from photo-reduction of acidic Cu-containing wastewater and its reuse as a catalyst,” *J. Water Process Eng.*, vol. 32, p. 100958, Dec. 2019.
- [45] D. Ferrah and P. Tieu, “Controllable Growth of Copper on TiO₂ Nanoparticles by Photodeposition Based on Coupled Effects of Solution Viscosity and Photoreduction Rate for Catalysis-Related Applications,” *ACS Appl. Nano Mater.*, vol. 3, no. 6, pp. 5855–5861, Jun. 2020.
- [46] V. Polliotto *et al.*, “Copper-Modified TiO₂ and ZrTiO₄: Cu Oxidation State Evolution during Photocatalytic Hydrogen Production,” *ACS Appl. Mater. Interfaces*, vol. 10, no. 33, pp. 27745–27756, Aug. 2018.
- [47] P. Cheng *et al.*, “TiO₂ e graphene nanocomposites for photocatalytic hydrogen production from splitting water,” *Int. J. Hydrogen Energy*, vol. 37, no. 3, pp. 2224–2230, 2011.

- [48] D. D'Elia *et al.*, "Impact of three different TiO₂ morphologies on hydrogen evolution by methanol assisted water splitting: Nanoparticles, nanotubes and aerogels," *Int. J. Hydrogen Energy*, vol. 36, no. 22, pp. 14360–14373, 2011.
- [49] Y. Gong *et al.*, "New insights into the photocatalytic activity of 3-D core-shell P25@silica nanocomposites: impact of mesoporous coating," *Dalt. Trans.*, vol. 46, no. 15, pp. 4994–5002, 2017.
- [50] S. Filice *et al.*, "Laser processing of TiO₂ colloids for an enhanced photocatalytic water splitting activity," *J. Colloid Interface Sci.*, vol. 489, pp. 131–137, 2017.
- [51] S. G. Sanches, J. H. Flores, and M. I. Pais da Silva, "Influence of Ti source on the Ti-HMS photocatalyst synthesis used in a water splitting reaction," *Mater. Res. Bull.*, vol. 109, no. April 2018, pp. 82–89, 2019.
- [52] G. D. Gesesse *et al.*, "Enhanced Photogenerated Charge Carriers and Photocatalytic Activity of Biotemplated Mesoporous TiO₂ Films with a Chiral Nematic Structure," *Chem. Mater.*, vol. 31, no. 13, pp. 4851–4863, Jun. 2019.
- [53] U. G. Akpan and B. H. Hameed, "Parameters affecting the photocatalytic degradation of dyes using TiO₂ -based photocatalysts : A review," vol. 170, pp. 520–529, 2009.
- [54] D. Praveen Kumar *et al.*, "Nano-size effects on CuO/TiO₂ catalysts for highly efficient H₂ production under solar light irradiation.," *Chem. Commun. (Camb).*, vol. 49, no. 82, pp. 9443–5, 2013.
- [55] H. A. Hamad, W. A. Sadik, M. M. Abd El-latif, A. B. Kashyout, and M. Y. Feteha, "Photocatalytic parameters and kinetic study for degradation of dichlorophenol-indophenol (DCPIP) dye using highly active mesoporous TiO₂ nanoparticles," *J. Environ. Sci. (China)*, vol. 43, pp. 26–39, 2016.

- [56] A. Lais, M. A. Gondal, M. A. Dastageer, and F. F. Al-Adel, "Experimental parameters affecting the photocatalytic reduction performance of CO₂ to methanol: A review," *Int. J. Energy Res.*, vol. 42, no. 6, pp. 2031–2049, May 2018.
- [57] S. N. Habisreutinger, L. Schmidt-Mende, and J. K. Stolarczyk, "Photocatalytic reduction of CO₂ on TiO₂ and other semiconductors," *Angew. Chemie - Int. Ed.*, vol. 52, no. 29, pp. 7372–7408, 2013.
- [58] A. Olivo *et al.*, "CO₂ photoreduction with water: Catalyst and process investigation," *Biochem. Pharmacol.*, vol. 12, pp. 86–94, 2015.
- [59] A. Ahmed, N. S. Gajbhiye, and A. G. Joshi, "Low cost, surfactant-less, one pot synthesis of Cu₂O nano-octahedra at room temperature," *J. Solid State Chem.*, vol. 184, no. 8, pp. 2209–2214, 2011.
- [60] M. Zanatta *et al.*, "Cu₂O/TiO₂ heterostructures on a DVD as easy&cheap photoelectrochemical sensors," *Thin Solid Films*, vol. 603, pp. 193–201, 2016.
- [61] F. Plascencia-Hernández *et al.*, "Cu₂O cubic and polyhedral structures versus commercial powder: Shape effect on photocatalytic activity under visible light," *J. Saudi Chem. Soc.*, vol. 23, no. 8, pp. 1016–1023, 2019.
- [62] K. Chalastara, F. Guo, S. Elouatik, and G. P. Demopoulos, "Tunable Composition Aqueous-Synthesized Mixed-Phase TiO₂ Nanocrystals for Photo-Assisted Water Decontamination: Comparison of Anatase, Brookite and Rutile Photocatalysts," *Catalysts*, vol. 10, no. 4, p. 407, Apr. 2020.
- [63] M. Muscetta, R. Andreozzi, L. Clarizia, I. Di Somma, and R. Marotta, "Hydrogen production through photoreforming processes over Cu₂O/TiO₂ composite materials: A mini-review," *Int. J. Hydrogen Energy*, vol. 45, no. 53, pp. 28531–28552, Oct. 2020.
- [64] J. Low, B. Cheng, and J. Yu, "Surface modification and enhanced photocatalytic CO₂ reduction

- performance of TiO₂: a review,” *Appl. Surf. Sci.*, vol. 392, pp. 658–686, 2017.
- [65] Y. Wang *et al.*, “Surfactant-free synthesis of Cu₂O hollow spheres and their wavelength-dependent visible photocatalytic activities using LED lamps as cold light sources.,” *Nanoscale Res. Lett.*, vol. 9, no. 1, p. 624, 2014.
- [66] K. Kaviyarasan, V. Vinoth, T. Sivasankar, A. M. Asiri, J. J. Wu, and S. Anandan, “Photocatalytic and photoelectrocatalytic performance of sonochemically synthesized Cu₂O@TiO₂ heterojunction nanocomposites,” *Ultrason. Sonochem.*, vol. 51, no. October 2018, pp. 223–229, 2019.
- [67] D. Y. C. Leung *et al.*, “Hydrogen production over titania-based photocatalysts,” *ChemSusChem*, vol. 3, no. 6, pp. 681–694, 2010.
- [68] S. C. Roy, O. K. Varghese, M. Paulose, and C. a Grimes, “Toward Solar Fuels : Photocatalytic Hydrocarbons,” *ACS Nano*, vol. 4, no. 3, pp. 1259–1278, 2010.
- [69] Q. Zhang *et al.*, “CuO nanostructures: Synthesis, characterization, growth mechanisms, fundamental properties, and applications,” *Prog. Mater. Sci.*, vol. 60, no. 1, pp. 208–237, 2014.
- [70] Y. Lan, Y. Lu, and Z. Ren, “Mini review on photocatalysis of titanium dioxide nanoparticles and their solar applications,” *Nano Energy*, vol. 2, no. 5, pp. 1031–1045, 2013.
- [71] J. Low, B. Cheng, and J. Yu, “Surface modification and enhanced photocatalytic CO₂ reduction performance of TiO₂: a review,” *Appl. Surf. Sci.*, vol. 392, pp. 658–686, 2016.
- [72] Y. Shi, Z. Yang, B. Wang, H. An, Z. Chen, and H. Cui, “Adsorption and photocatalytic degradation of tetracycline hydrochloride using a palygorskite-supported Cu₂O-TiO₂ composite,” *Appl. Clay Sci.*, vol. 119, pp. 311–320, 2016.
- [73] E. Szaniawska, K. Bienkowski, I. A. Rutkowska, P. J. Kulesza, and R. Solarska, “Enhanced photoelectrochemical CO₂-reduction system based on mixed Cu₂O – nonstoichiometric TiO₂ photocathode,” *Catal. Today*, vol. 300, no. May, pp. 145–151, 2018.

- [74] Y. Wang *et al.*, “A unique Cu₂O/TiO₂ nanocomposite with enhanced photocatalytic performance under visible light irradiation,” *Ceram. Int.*, vol. 43, no. 6, pp. 4866–4872, 2017.
- [75] Y. Wei *et al.*, “Synergistic impact of cocatalysts and hole scavenger for promoted photocatalytic H₂ evolution in mesoporous TiO₂–NiS x hybrid,” *J. Energy Chem.*, vol. 32, pp. 45–56, May 2019.
- [76] T. Iwasita, “Electrocatalysis of methanol oxidation,” *Electrochim. Acta*, vol. 47, no. 22–23, pp. 3663–3674, Aug. 2002.
- [77] T. M. D. Dang, T. T. T. Le, E. Fribourg-Blanc, and M. C. Dang, “Synthesis and optical properties of copper nanoparticles prepared by a chemical reduction method,” *Adv. Nat. Sci. Nanosci. Nanotechnol.*, vol. 2, no. 1, p. 015009, Mar. 2011.
- [78] P. Pootawang, N. Saito, and S. Y. Lee, “Discharge time dependence of a solution plasma process for colloidal copper nanoparticle synthesis and particle characteristics,” *Nanotechnology*, vol. 24, no. 5, p. 055604, Feb. 2013.
- [79] S. Venkatakrishnan, G. Veerappan, E. Elamparuthi, and A. Veerappan, “Aerobic synthesis of biocompatible copper nanoparticles: promising antibacterial agent and catalyst for nitroaromatic reduction and C–N cross coupling reaction,” *RSC Adv.*, vol. 4, no. 29, pp. 15003–15006, Mar. 2014.
- [80] G. Yu *et al.*, “Electrodeposition of submicron/nanoscale Cu₂O/Cu junctions in an ultrathin CuSO₄ solution layer,” *J. Electroanal. Chem.*, vol. 638, no. 2, pp. 225–230, Jan. 2010.
- [81] Z. Xi, C. Li, L. Zhang, M. Xing, and J. Zhang, “Synergistic effect of Cu₂O/TiO₂ heterostructure nanoparticle and its high H₂ evolution activity,” *Int. J. Hydrogen Energy*, vol. 39, no. 12, pp. 6345–6353, 2014.
- [82] A. L. Linsebigler, A. L. Linsebigler, J. T. Yates Jr, G. Lu, G. Lu, and J. T. Yates, “Photocatalysis

on TiO₂ Surfaces: Principles, Mechanisms, and Selected Results,” *Chem. Rev.*, vol. 95, no. 3, pp. 735–758, 1995.

- [83] K. Rajeshwar, N. R. de Tacconi, G. Ghadimkhani, W. Chanmanee, and C. Janáky, “Tailoring Copper Oxide Semiconductor Nanorod Arrays for Photoelectrochemical Reduction of Carbon Dioxide to Methanol,” *ChemPhysChem*, vol. 14, no. 10, pp. 2251–2259, Jul. 2013.
- [84] B. Ohtani, O. O. Prieto-Mahaney, D. Li, and R. Abe, “What is Degussa (Evonic) P25? Crystalline composition analysis, reconstruction from isolated pure particles and photocatalytic activity test,” *J. Photochem. Photobiol. A Chem.*, vol. 216, no. 2–3, pp. 179–182, Dec. 2010.
- [85] L. Clarizia *et al.*, “Effect of surface properties of copper-modified commercial titanium dioxide photocatalysts on hydrogen production through photoreforming of alcohols,” *Int. J. Hydrogen Energy*, vol. 42, no. 47, pp. 28349–28362, Nov. 2017.